Influence of sea ice on the atmosphere: A study with an Arctic atmospheric regional climate model

Article *in* Journal of Geophysical Research Atmospheres · August 2006

DOI: 10.1029/2005JD006957

CITATIONS
40

READS
78

4 authors:

Annette Rinke
Alfred Wegener Institute Helmholtz Centre for Polar and Marine Research
163 PUBLICATIONS **5,616** CITATIONS
SEE PROFILE

Wieslaw Maslowski
Naval Postgraduate School
119 PUBLICATIONS **2,860** CITATIONS
SEE PROFILE

Klaus Dethloff
Alfred Wegener Institute Helmholtz Centre for Polar and Marine Research
198 PUBLICATIONS **4,424** CITATIONS
SEE PROFILE

Jaclyn Clement Kinney
Naval Postgraduate School
45 PUBLICATIONS **794** CITATIONS
SEE PROFILE

Influence of sea ice on the atmosphere: A study with an Arctic atmospheric regional climate model

Annette Rinke,[1] Wieslaw Maslowski,[2] Klaus Dethloff,[1] and Jaclyn Clement[2]

Received 6 December 2005; revised 19 April 2006; accepted 22 May 2006; published 18 August 2006.

[1] The impact of the lower-boundary forcing over ocean grid points, namely of sea surface temperature (SST), sea ice fraction, and sea ice thickness, on the mean atmospheric simulation is investigated with an Arctic atmospheric regional climate model. The assessment shows that the sea ice/SST forcing has an impact on the atmospheric simulations. The near-surface air temperature response shows a strong, seasonally dependent sensitivity to sea ice changes. The response is small in summer but significant in winter, and changes in the marginal ice zone have the largest impact on the atmosphere. During winter, the realistic representation of the marginal sea ice zone is important as it contributes to the simulation of regional atmospheric circulation patterns and temperature profiles. Changes in sea ice thickness of the western Arctic lower boundary indicate an Arctic-wide response in the large-scale circulation and seem to have an impact on the troposphere-stratosphere coupling. During summer the direct thermodynamic effect of sea ice changes is small, while the dynamic response is still of importance but smaller than in winter.

Citation: Rinke, A., W. Maslowski, K. Dethloff, and J. Clement (2006), Influence of sea ice on the atmosphere: A study with an Arctic atmospheric regional climate model, *J. Geophys. Res.*, *111*, D16103, doi:10.1029/2005JD006957.

1. Introduction

[2] Sea ice plays a critical role in the Arctic climate system [*Arctic Climate Impact Assessment*, 2005], because of its reflective surface affecting the albedo associated with the ice-albedo-temperature feedback, and its impact on the transfer of heat, moisture and momentum between the ocean and atmosphere and associated feedbacks involving humidity and clouds. In winter, sea ice insulates the relatively warm ocean water from the cold polar atmosphere except where cracks or leads in the ice and polynyas allow exchange of heat and water vapor from ocean to atmosphere. The number of leads and polynyas determines where and how much heat and water are lost to the atmosphere, which may affect the local cloud cover and precipitation. In the marginal ice zones like in the Barents Sea, the oceanic heat loss in winter can reach more than 600 W/m^2 [*Harms et al.*, 2005], which presents a significant input to the local atmosphere. However, the impact of Arctic sea ice cover changes on the atmospheric circulation may not be limited to local or Arctic-wide, but could have global implications. *Dethloff et al.* [2006] discuss feedbacks that occur through the modulation of the strength of subpolar westerlies and storm tracks. Our understanding of extratropical atmosphere-ocean interactions, focusing on the atmospheric response to sea surface temperature (SST) anomalies has been advanced during the last several years (see *Kushnir et al.* [2002] for a synthesis and evaluation, and recently, *Deser et al.* [2004] and *Alexander et al.* [2004]). SST/sea ice anomalies directly affect a local thermal forcing to the atmosphere, which in turn induces a local modification of the geopotential height field. The geostrophic adjustment implies the development of an anomaly of the vorticity field which then propagates through the dispersion of stationary Rossby waves.

[3] In this sense, the specification of lower-boundary conditions in a regional climate model (RCM) is crucial to overall simulations. Generally, the lateral boundary conditions exert a strong control on RCM simulations, however this control is weaker in a large circumpolar Arctic domain, which allows more internal variability and the development of nonlinear interactions. Very few Arctic RCM studies have investigated the impact of lower-boundary forcing (i.e., of the prescribed sea ice/SST on the regional atmospheric circulation) and these were case studies, which are not systematic [*Rinke and Dethloff*, 2000; *Görgen*, 2004; *Semmler et al.*, 2004]. This paper presents an approach in which an atmosphere stand-alone RCM is exposed to different sea ice/SST data sets at its lower boundary. The applied forcing conditions do not describe selected idealized cases but represent "realistic" conditions. One data set is the commonly used European Centre for Medium-Range Weather Forecasts (ECMWF) reanalysis data set, while the other comes from a state-of-the-art coupled ice-ocean model driven by the ECMWF reanalysis atmospheric data. By comparing the two atmospheric RCM simulations driven by different lower-boundary forcing (but driven by the same

[1] Alfred Wegener Institute for Polar and Marine Research, Potsdam, Germany.
[2] Department of Oceanography, Naval Postgraduate School, Monterey, California, USA.

0148-0227/06/2005JD006957

lateral forcing), the impact of inaccurate sea ice/SST information on the atmospheric simulation will be discussed. Especially inaccurate is the assumption of a fixed sea ice thickness (most Arctic RCMs use a uniform thickness of 2 m). The aim of this investigation is to quantify the atmospheric climatological mean response to a different lower-boundary forcing and to identify those cases where a more accurate lower-boundary forcing seems necessary for realistic atmospheric simulations.

[4] The specific approach, the employed RCM and the experimental design of the 15- yearlong simulations are described in section 2. Results are presented sequentially in section 3: the differences between the two applied SST/sea ice forcing data sets in section 3.1. and the impact on surface variables and atmospheric structure in sections 3.2–3.3. Section 4 summarizes the results and presents conclusions.

2. Approach

[5] The state-of-the-art atmospheric RCM HIRHAM [*Christensen et al.*, 1996; *Dethloff et al.*, 1996] has been configured for the pan-Arctic domain and 15-yearlong simulations over the period of 1979–1993 have been performed. The influence of the actual sea ice conditions has been investigated by conducting two HIRHAM simulations differing only by the SST and sea ice data set applied at the lower boundary during the simulation.

[6] One widely used data set is that from the ERA15 reanalysis [*Gibson et al.*, 1997] from the ECMWF. ERA15 data cover the period 1979–1993 and have a horizontal spectral resolution of T106 (Gaussian grid resolution 1.125° or about 125 km). From November 1981 onward, NCEP weekly SST data were used for the reanalysis, while GISST data were used prior to November 1981. Both data sets have a 1 degree resolution. There is no separate field in ERA15 describing the sea ice cover; it was derived from the SSTs. If SST is warmer (colder) than −1.0°C (−1.8°C), then the sea ice fraction is set to 0 (1), and for SSTs in between, a fractional ice mask is parameterized [*Christensen et al.*, 1996]. Using ice fraction data derived this way, a constant ice thickness of 2 m is set everywhere where ice fraction is greater than 0.5.

[7] The second SST/sea ice data set is from the Naval Postgraduate School (NPS) coupled ice-ocean model, which was run over the same 15 years, driven by daily ERA15 atmospheric data (2m air and dew point temperatures, 10 m winds, surface incoming long- and shortwave radiation) [*Maslowski et al.*, 2004; *Clement et al.*, 2005]. The coupled model adapts the Los Alamos National Laboratory (LANL) Parallel Ocean Program (POP) ocean model with a free surface formulation [*Dukowicz and Smith*, 1994]. The sea ice model uses a viscous-plastic rheology, the zero-layer approximation of heat conduction through ice and a simplified surface energy budget [*Zhang et al.*, 1999; *Maslowski and Lipscomb*, 2003]. Both components of the coupled model use identical rotated spherical coordinate grids, configured at 1/12° (1280 by 720 points in the horizontal and 45 levels in the vertical direction). The model domain includes the Arctic, North Atlantic down to 40°N, and North Pacific down to 30°N. A 73 year integration has been completed, including a 48 year spin-up and a 25 year interannual run forced with daily averaged ECMWF atmospheric fields, including 1979–1993 reanalysis data and 1994–2003 operational products. In addition, to correct for the missing fluxes between the ocean and overlying atmosphere or sea ice (namely P-E and additional runoff, including glacier meltwater inflow into Gulf of Alaska, Greenland ice sheet meltwater, runoff into the Baltic Sea, Hudson Bay and discharge from many smaller rivers) the ocean surface level, 5 m thick, is restored on a monthly timescale to the monthly temperature and salinity fields from the Polar Science Center Hydrographic Climatology (PHC) [*Steele et al.*, 2001]. The NPS ice-ocean model results have shown long-term and large-scale variability in the ocean freshwater and Atlantic Water circulation and sea ice conditions between the 1970/80s and 1990s [*Maslowski et al.*, 2000, 2001] in qualitative agreement with measurements from icebreaker expeditions and submarine data collected during the 1990s.

2.1. Atmospheric Regional Climate Model HIRHAM

[8] HIRHAM has already been applied on the pan-Arctic domain for a wide range of applications (recently, e.g., *Rinke et al.* [2004a] and *Dethloff et al.* [2004]). The integration domain covers the entire Arctic north of ~65°N (see Figure 1) with 110 by 100 grid points and a horizontal resolution of 0.5 degrees. The vertical discretization consists of 19 irregularly spaced levels. HIRHAM contains the physical parameterization package of the general circulation model ECHAM4 [*Roeckner et al.*, 1996], which includes radiation, cumulus convection, planetary boundary layer and land surface processes, and gravity wave drag. A time step of 5 min is used. The model is forced at the lateral boundaries by temperature, wind, humidity, and surface pressure (updated every 6 hours). At the lower boundary over land grid points, the soil temperatures and water are initialized according to climatology and afterward are calculated every time step using the energy and water budget equations. At the ocean lower boundary, the model is forced by SST, sea ice fraction and thickness (updated daily). The sea ice surface temperature is calculated prognostically via a heat balance equation linearized in both temperature and time. Sea ice is treated by a scheme adapted from the Ocean Isopycnal Model (OPYC) [*Oberhuber*, 1992] taking into account fraction and thickness of sea ice. Sea ice affects the atmospheric simulation in the model via two main processes: the atmosphere-ocean heat exchange and the albedo effect. In the boundary layer scheme, the effects of fractional sea ice cover on the roughness length and on turbulent heat fluxes are included. In the radiation scheme, a grid cell-averaged surface albedo is used, which is calculated according to the following formulation: $A = f_{ice} A_{ice} + (1 - f_{ice}) A_{sea}$, i.e., for a grid cell partially ice covered (portion f_{ice}), the surface albedo consists of an ice albedo A_{ice} and an albedo of open sea A_{sea} which is fixed to 0.07. The ice albedo is surface temperature–dependent and accounts for meltwater ponds on ice near the melting point. The prescribed sea ice thickness influences the thermal conduction through the ice. More detailed descriptions of these parameterizations are given by *Roeckner et al.* [1996].

2.2. Experimental Design

[9] Two 15-yearlong HIRHAM simulations have been performed, each over the ERA15 time period 1979–1993.

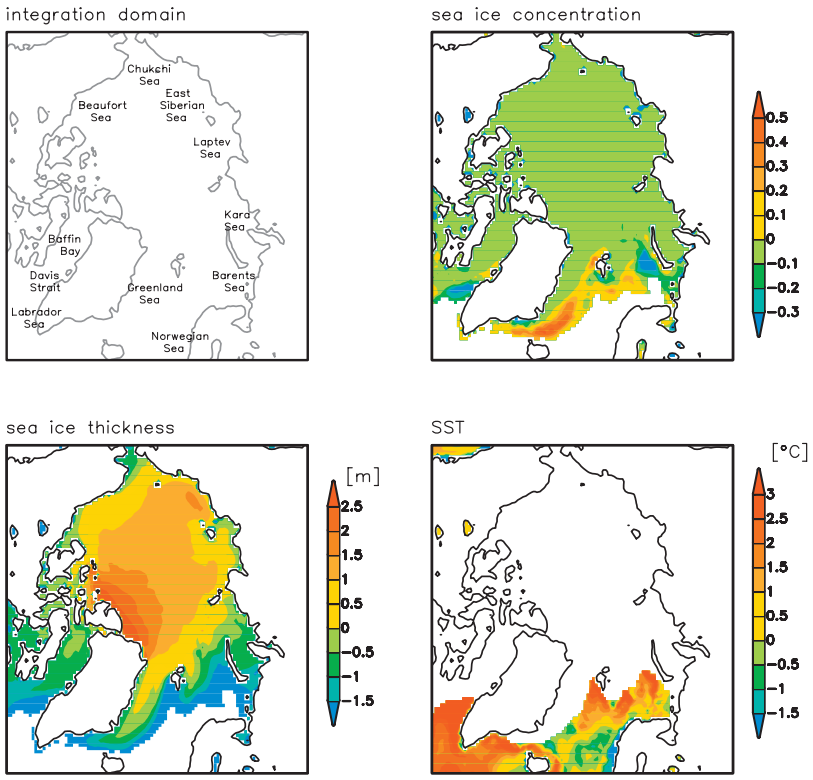

Figure 1. Integration domain and differences of sea ice concentration, thickness, and sea surface temperature (SST) between the data computed from the Naval Postgraduate School (NPS) ice-ocean model and ERA15 data ("NPS minus ERA15"), for mean winter (DJF) 1979–1993.

The lateral boundary forcing data are exactly the same in both HIRHAM runs and are provided by the 6 hourly ERA15 data. The lower-boundary forcing data are updated daily, and represent the only difference between the two HIRHAM runs. The applied lower-boundary forcing data sets are (1) SST and sea ice fraction from the ERA15 data, and the sea ice thickness is fixed to 2 m for all sea ice grid points, and (2) SST, sea ice fraction, and sea ice thickness from the NPS ice-ocean model output. The two HIRHAM simulations are called "HIRHAM.era" and "HIRHAM.nps," respectively.

3. Results

[10] Climatological seasonal means 1979–1993 have been calculated from the HIRHAM output. The simulations have been analyzed with special emphasis on winter (DJF), when the latent and sensible heat fluxes for open waters are large and the incoming shortwave radiative flux is low. During that season, changes in sea ice concentration and/or thickness are expected to have the largest impact on the atmospheric heat fluxes because the near-surface air and ocean temperatures differ largely. However, this paper also presents the seasonal cycle of the atmospheric response to the modified lower-boundary forcing.

3.1. Forcing Differences

[11] In this section, the differences between the two SST/sea ice data sets are discussed. Figure 1 shows the differences in SST, sea ice fraction, and sea ice thickness for mean winter conditions. The most significant SST differences are found in the Labrador and Barents Seas where the NPS data set is up to 3°C warmer than the ERA15 data. Associated with this, the NPS model simulates less ice concentration in these two regions. However, we note that the NPS results are obtained with the surface restoring to the monthly PHC temperature and salinity climatology, which acts to keep these surface parameters within a range of climatological values (for more discussion, see *Steele et al.* [2001]). The fact that SSTs differ most within the marginal ice zones in the Barents and Labrador Seas suggests that some of the SST differences can be attributed to smoothing of limited and low-resolution observations in those regions compared to the analyzed, more detailed (at 9 km and monthly mean values) model results. In particular, comparison of the NPS model mean summer and winter sea ice concentration, surface temperature and salinity fields in the Barents Sea with the National Oceanic and Atmospheric Administration Barents Sea Climatic Atlas [*Matishov et al.*, 1998] reveals that such features as the North Cape Current, the location of the Barents Sea Polar Front, and the northward extent of warm surface Atlantic Water toward the St. Anna Trough agree well with the climatology [*Maslowski et al.*, 2004]. Similar arguments can be applied in the northern Labrador Sea, however the influence of model lateral boundary conditions in the North Atlantic on warmer SSTs in the southern Labrador Sea cannot be excluded. The argument about oversmoothed ERA15 SST/sea ice climatology data can be clearly seen along the sea ice edge in the Greenland, Iceland, and Irminger seas (Figure 1), where (model) higher sea ice concentrations

Table 1. Root-Mean-Square Differences of Atmospheric Variables Between Both Simulations HIRHAM.nps and HIRHAM.era for the Mean Seasons (Averaged Over 1979–1993)[a]

	DJF	MAM	JJA	SON
Sea level pressure, hPa	0.46 (0.60)	0.55 (0.73)	0.26 (0.34)	0.39 (0.50)
2 m air temperature, K	2.2 (2.9)	1.4 (1.9)	0.9 (1.3)	1.2 (1.6)
Latent heat flux, W/m^2	13.0 (17.3)	10.3 (11.4)	7.9 (10.5)	7.3 (9.9)
Sensible heat flux, W/m^2	23.9 [31.7]	12.0 (16.2)	5.5 (7.5)	8.8 (11.9)
Total cloud cover, %	5.0 (6.4)	2.8 (3.6)	3.7 (5.2)	2.4 (3.0)
Precipitation, mm	27 (38)	17 (24)	17 (23)	15 (21)

[a]The values are for the pan-Arctic domain and in parentheses for the ocean grid points only.

occur at the same locations where (model) higher SSTs exist. In reality, one would expect that warmer SSTs should yield lower (not higher) sea ice concentrations.

[12] Figure 1 further shows that the sea ice thickness differences between the two data sets are 0.5–2.5 m in the central Arctic. The spatial sea ice thickness pattern simulated by the NPS model closely represents the observed pattern [*Bourke and Garrett*, 1987; *Bourke and McLaren*, 1992] with maximum sea ice thickness over 5 m near the northern Canadian Archipelago and Greenland and an average sea ice thickness from 3.0 to 3.5 m in the central Arctic Ocean [*Maslowski and Lipscomb*, 2003; *Preller et al.*, 2002]. Although the uniformly prescribed 2 m sea ice thickness in the HIRHAM.era run is not realistic, it is commonly used in atmospheric Arctic RCM simulations.

[13] It is assumed that the sea ice forcing contributes significantly to the atmospheric response, since changes in sea ice cover have a larger impact on the surface energy fluxes than SST changes of a few degrees in already-open sea areas. Furthermore, earlier studies have demonstrated only a weak response to North Atlantic SST anomalies [*Kushnir et al.*, 2002; *Paeth et al.*, 2003]. However, it appears that the Labrador Sea SSTs have a stronger influence on the atmospheric circulation, compared to SSTs in other parts of the northern North Atlantic basin [*Lopez et al.*, 2000]. Furthermore, *Singarayer et al.* [2005] suggest that the specification of ice extent is less critical than the areas of open water within the ice cover.

3.2. Impact on Surface Variables

[14] Atmospheric conditions, such as air temperature, turbulent heat fluxes, cloud cover and precipitation, are crucially dependent on the sea ice/SST conditions. In the following sections, these sensitivities are discussed and summarized in Table 1.

3.2.1. Spatial Patterns of Surface Variables

[15] The different SST and sea ice fields at the lower model boundary in the HIRHAM runs lead to strong changes in both the latent and sensible heat fluxes at the ocean surface. The total heat flux difference is a quite linear function of the sea ice fraction difference (Figure 2). Large (small) changes of sea ice fraction lead to large (small) heat flux changes. A sea ice fraction difference of 0.5 is associated with a heat flux change of 100–150 W/m^2.

[16] Figure 3 presents ''HIRHAM.nps minus HIRHAM.era'' differences of several variables for mean

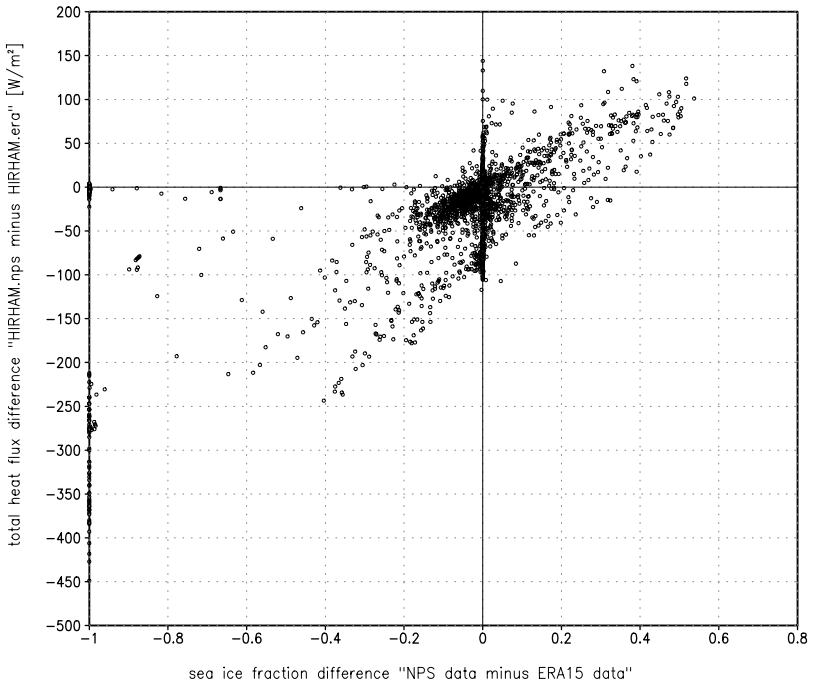

Figure 2. Dependency of the total (latent + sensible) heat flux change on the sea ice fraction change for DJF 1979–1993. The individual dots are for each individual ocean grid point.

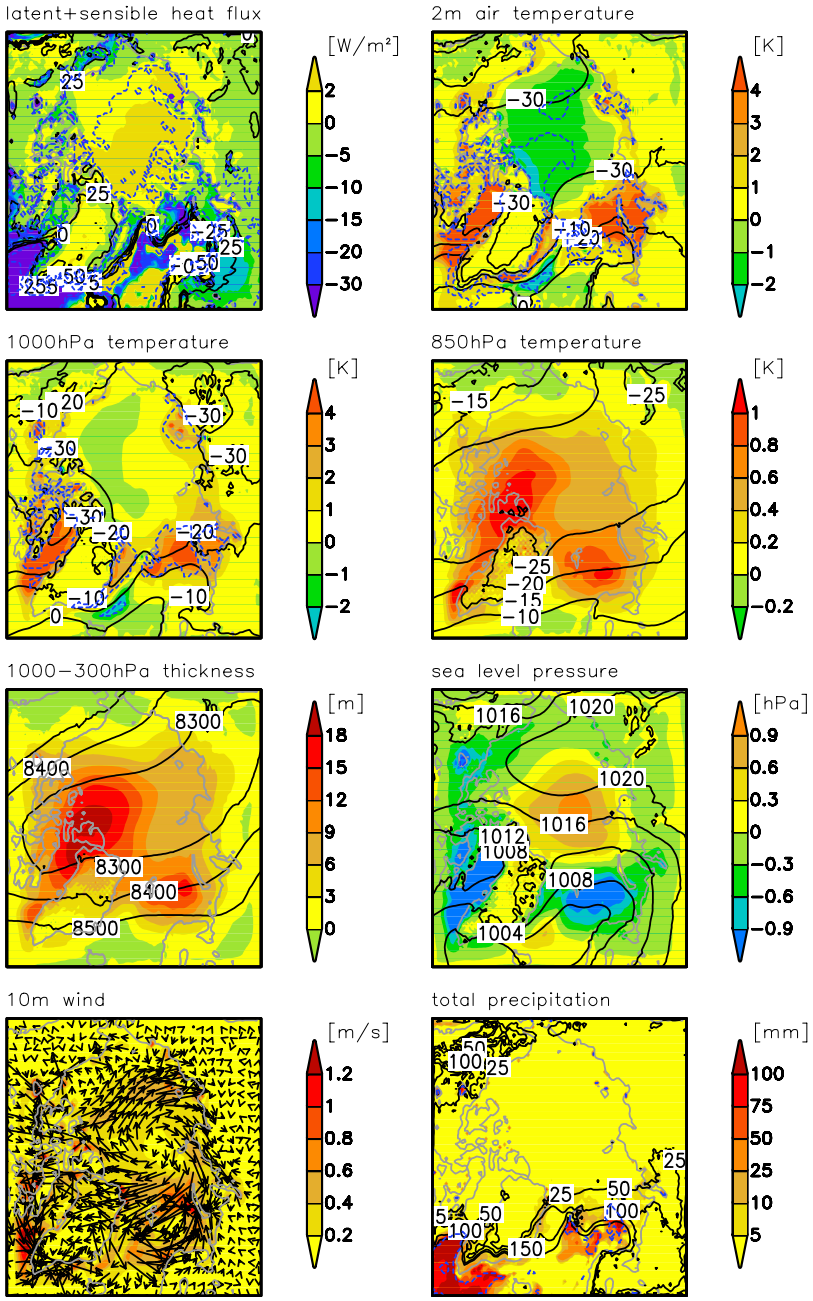

Figure 3. Differences "HIRHAM.nps minus HIRHAM.era" (color shading) and HIRHAM.era (isolines) for DJF 1979–1993. The sign convention for the heat fluxes is such that negative fluxes indicate an upward flux of heat into the atmosphere. Dashed blue contours represent the lower limit for 95% significance. The 10 m wind picture shows the differences of the wind speed (color shading) and the wind vector.

winter associated with the different sea ice/SST forcing. The statistical significance of the differences has been evaluated with a *t*-test (two-sided Student's *t*-test applied to each individual grid point; the lower limit for 95% significance is presented as dashed contours). The strongest impacts of SST changes on the surface heat fluxes are expected at places where SST changes induce modifications of the sea ice cover as the turbulent heat flux is dependent on the air-sea temperature difference and low-level wind speed and humidity. The most remarkable heat flux changes occur in the Labrador and Barents Seas. HIRHAM.nps simulates much stronger upward heat fluxes compared to HIRHAM.era. Both sensible and latent heat fluxes in the Labrador Sea are up to 50 W/m^2 stronger, which is an increase by ca. 30% (relative to the HIRHAM.era value). Similarly, enhanced upward heat fluxes occur in the Barents Sea with changes up to 80 W/m^2 (i.e., an increase by ca. 80%). The albedo is lowered in those parts of the Labrador and Barents Seas where NPS data show less ice fraction and more open water and this is associated with

enhanced absorption of shortwave radiation at the surface. This strong surface heating contributes to greater turbulent heat fluxes from the ocean into the atmosphere. In line with the slightly colder SSTs in the northern North Atlantic (Norwegian Sea) in HIRHAM.nps, the upward heat fluxes are weaker (by about 5 W/m^2) compared with HIRHAM.era. Over the central Arctic Ocean, the heat flux changes are very small (weaker upward fluxes in HIRHAM.nps; 0.05–0.2 W/m^2 change in latent heat flux and 1.5–2.5 W/m^2 change in sensible heat flux) according to the sea ice thickness differences and very small sea ice fraction changes.

[17] The heat flux changes are expected to modify the local near-surface temperature. Associated with the warmer SST and reduced sea ice concentrations/thickness, and therefore stronger upward heat fluxes in the Labrador Sea/Davis Strait and Barents Sea, HIRHAM.nps simulates warmer (by about 4 K) 2m air temperatures (in the following abbreviated with 2mT) than HIRHAM.era. The performed *t*-test shows that the 2mT differences are significant at the 95% confidence level in the Barents/Labrador Seas and east/west of Greenland. Compared with the magnitude of simulation uncertainty due to imperfect initial and lateral boundary conditions, these magnitudes of 2mT differences are significant [*Rinke et al.*, 2004b, Figures 3 and 8].

[18] In contrast, the 2mT over the central Arctic Ocean is slightly colder (by 1–2 K) in HIRHAM.nps which can be attributed to the thicker sea ice and reduced upward heat fluxes there. Accordingly, the maximum cooling of 2–3 K occurs along the northern Canadian Archipelago (i.e., the area of thickest ice). At a height of 1000 hPa, a slight cooling over this region is still apparent, however a predominant warming is already recognized. At a height of 850 hPa, the warming has been spread over the whole Arctic domain, and now shows a maximum warming over the western Arctic (centered over the Canadian Archipelago) and a secondary maximum over the Barents Sea. Figure 3 further shows that the whole troposphere has been warmed Arctic-wide. The mean tropospheric temperature is expressed here by the 1000–300 hPa geopotential thickness. The two local maxima of the mean tropospheric warming (positive geopotential thickness anomaly) are found in the western Arctic near the Canadian Archipelago and over the Barents Sea. The latter is clearly connected with the large local surface warming, while the former points to advective processes. This result shows that the introduced SST/sea ice changes cause both a direct local surface heating (and therefore atmospheric warming located over the SST/sea ice anomaly region) and an indirect atmospheric warming over regions characterized by no local surface heating. The mechanism for the indirect effect is the advection of anomalies from the two warm region into the cold surface anomaly region, and expresses the coupling between the surface, very shallow boundary layer and free atmosphere. The maxima of the tropospheric thickness increase (and thus warming) are about 20 m and 15 m, respectively. A study by *Lopez et al.* [2000] showed that the magnitude of the thickening of the troposphere to warm Atlantic SST anomalies depends strongly on the applied SST geographical anomaly pattern. In the case of a generally warmer Atlantic, they simulated a similar thickening pattern as ours, however with an approximately 3 times stronger magnitude associated with their higher SST anomaly magnitudes.

[19] The warmer (colder) SST and 2mT are associated with reduced (increased) mean sea level pressure (SLP). The magnitudes of these SLP changes are on the order of 1 hPa, and the *t*-test does not show any significance. The magnitudes of the 2mT and SLP responses are of about the same order as in the recent GCM experiments of *Alexander et al.* [2004] and *Magnusdottir et al.* [2004]. The absolute SLP changes appear to be small (depending on the location, these are 1/3–1/6 of the observed interannual SLP variability calculated from ERA40 data of the time period 1979–2001) but the resulting pressure gradient changes induce pronounced 10 m wind changes (Figure 3).

[20] The differences in the latent heat fluxes are also reflected by differences in cloud cover and precipitation. In HIRHAM.nps, the cloud cover (not shown) and the precipitation are higher than in HIRHAM.era. Over the Atlantic, the precipitation is increased by up to 150 mm which is about a 50% increase, and the *t*-test confirmed the significance of the differences over the Atlantic, Labrador and Barents Seas at the 95% confidence level. Compared to the ERA40 data, both HIRHAM runs simulate higher precipitation in these ocean regions, but to draw a definitive conclusion is difficult due to the uncertainty of the data analysis over oceans.

[21] Increased areas of open water associated with increased heat fluxes into the atmosphere are known to have a significant impact on cyclone development [e.g., *Grønas*, 1995] and a warm surface anomaly can be considered as a positive potential vorticity anomaly, which can intensify existing cyclones [*Hoskins et al.*, 1985]. Accordingly, GCM investigations show distinct impacts of sea ice anomalies on storm tracks (recently, *Magnusdottir et al.* [2004], *Alexander et al.* [2004], and *Kvamsto et al.* [2004]). However, RCM case studies for the Laptev Sea and Fram Strait found only small influences of the lower-boundary specification on the synoptic activity [*Görgen*, 2004; *Semmler et al.*, 2004]. We present the interdiurnal variability (i.e., the absolute day-to-day changes) of SLP as a measure of the storm tracks (Figure 4). Figure 4 shows that the strongest transient cyclone activity during winter occurs along the west and east coasts of Greenland, and over the northern North Atlantic reaching as far as the Barents Sea. Further, it shows that the changed lower-boundary forcing leads only to very small changes in the storm tracks. The inspection of the 2–6 day bandpass-filtered standard deviation of SLP yields a similar result (not shown). A simple relationship between SST/sea ice changes and storm track changes could not be detected. This confirms the findings from the other RCM studies mentioned above and is probably related to the dominance of the lateral forcing.

[22] A logical next question is, Do the improved lower-boundary conditions lead to a better reproduction of the observed atmospheric conditions in the RCM? First, it must be emphasized that such a validation is especially difficult to obtain over the Arctic Ocean due to the limited availability of gridded observational data sets. Second, the RCM results depend strongly on the lateral and lower-boundary forcing. This means that if one compares both, the HIRHAM.era and HIRHAM.nps simulations with the ERA15 data, one could expect that HIRHAM.era is fa-

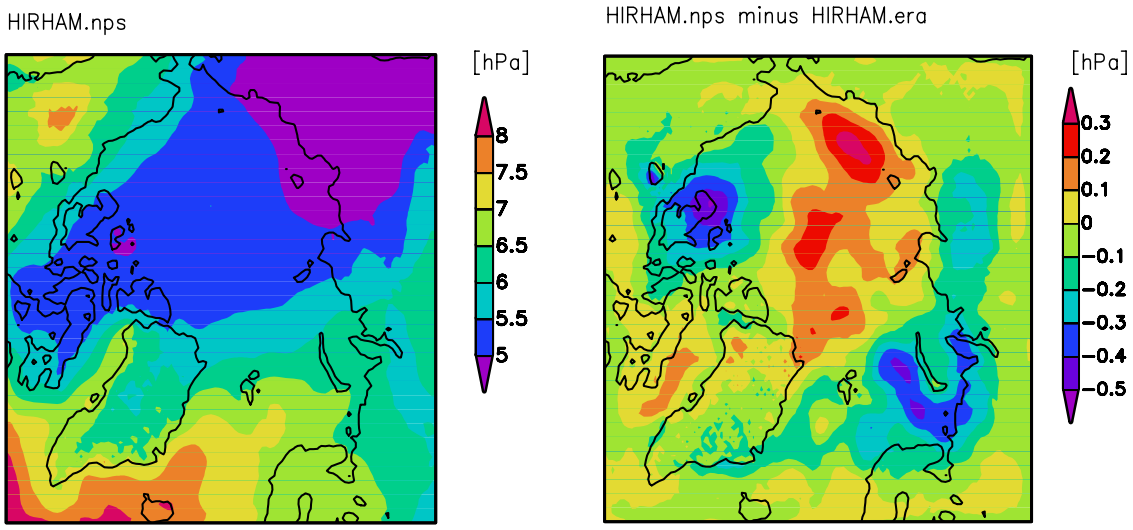

Figure 4. Interdiurnal variability of sea level pressure (SLP) for DJF 1979–1993. (left) HIRHAM.nps. (right) Difference "HIRHAM.nps minus HIRHAM.era."

voured to show better agreement as it was totally forced by the ERA15 data. However, it is an open question if this can be interpreted as a better agreement with reality (observations). Regardless of these difficulties, a validation attempt has been made for the 2mT and SLP results (Figure 5 and Table 2), and the two reanalysis data sets of ERA15 and ERA40 have been used for this comparison. Figure 5a demonstrates that the warmer 2mT in the Baffin Bay/Davis Strait, Kara Sea and parts of the Barents Sea in the HIRHAM.nps simulations are in better agreement with the ERA40 data than the HIRHAM.era results. The HIRHAM.nps simulated reduced SLP in the Baffin Bay/Davis Strait and Barents Sea are also in better agreement with the ERA40 data. The inspection of the differences between the ERA15 and ERA40 data (Figure 5b) indicates a close agreement over the Arctic Ocean, North Atlantic and adjacent seas (SLP differences are less than 1 hPa, and 2mT differences are less than 2 K), showing that these improvements in HIRHAM.nps do not depend on the selected reanalysis data set used for validation. Figure 5b shows a pronounced positive difference in 2m air temperature ("ERA40 minus ERA15") over land. This demonstrates the well-known fact that the ERA15 data are too cold over boreal forest compared with observations [*Viterbo and Betts*, 1999]. The root-mean-square error (RMSE) between the HIRHAM simulations and ERA data has been calculated for each of the 15 years and separately for the whole domain (Table 2) and ocean grid points only (not shown). Table 2 shows that the RMSE between the HIRHAM simulations and ERA40 data is generally smaller than between HIRHAM and ERA15 data. If the ERA15 data are considered for the validation, then for the 2mT, HIRHAM.era generally has a smaller RMSE than HIRHAM.nps. This is expected since the former simulation was driven totally by the ERA15 data. However, HIRHAM.nps has a better SLP agreement than HIRHAM.era (the RMSE is smaller in 11 of 15 years). Relative to the ERA40 data, the nps forcing leads to a smaller RMSE of SLP and 2mT in only about half of the years. The calculations for the ocean grid points give the similar results (not shown). For the 2mT validation, we also used the AVHRR Polar Pathfinder (APP) skin temperature data [*Fowler et al.*, 2002]. As these satellite-derived data are skin and clear-sky temperatures, and tend to be lower than the 2mT, they have been used only for the inspection of the spatial variability. For this, the pattern correlation coefficients between the seasonal HIRHAM and APP temperature patterns have been calculated for each year (not shown). The correlation coefficients are larger than 0.9 for all seasons and years, and are only slightly larger for HIRHAM.nps than for HIRHAM.era. Overall we conclude that the improved lower-boundary forcing contributes to only slightly improved atmospheric simulation.

3.2.2. Annual Cycle of Surface Variables

[23] This section considers the annual cycle of the boundary layer changes. Figure 6 presents the annual cycle of the difference "HIRHAM.nps minus HIRHAM.era" for the heat fluxes, 2mT, and SLP. To be able to attribute these atmospheric differences to specific sea ice differences, the variables have been averaged over grid points characterized by a certain sea ice thickness difference accordingly to Figure 1. For this, five classes of sea ice thickness differences "NPS minus ERA15" have been defined. Figure 6 shows that the 2mT differences are small during summer, independent of whether the sea ice thickness differences are small or large. This is explained by the small differences between ocean and near-surface air temperatures during summer and thus small turbulent heat fluxes. However, during winter there are significant 2mT differences with various sea ice differences. In those regions where sea ice is thicker (thinner), the near-surface air is colder (warmer). Changes in the marginal ice zone (red curve) have the largest impact on the atmosphere associated with large heat flux changes. The regions defined by sea ice thickness changes (x) of $x < -0.5$ m are also characterized by strong changes in sea ice concentrations (see Figure 1) which generate very large heat flux changes during winter. This indicates that changes in ice cover have stronger impacts on the heat fluxes than changes in ice thickness. Changes of the

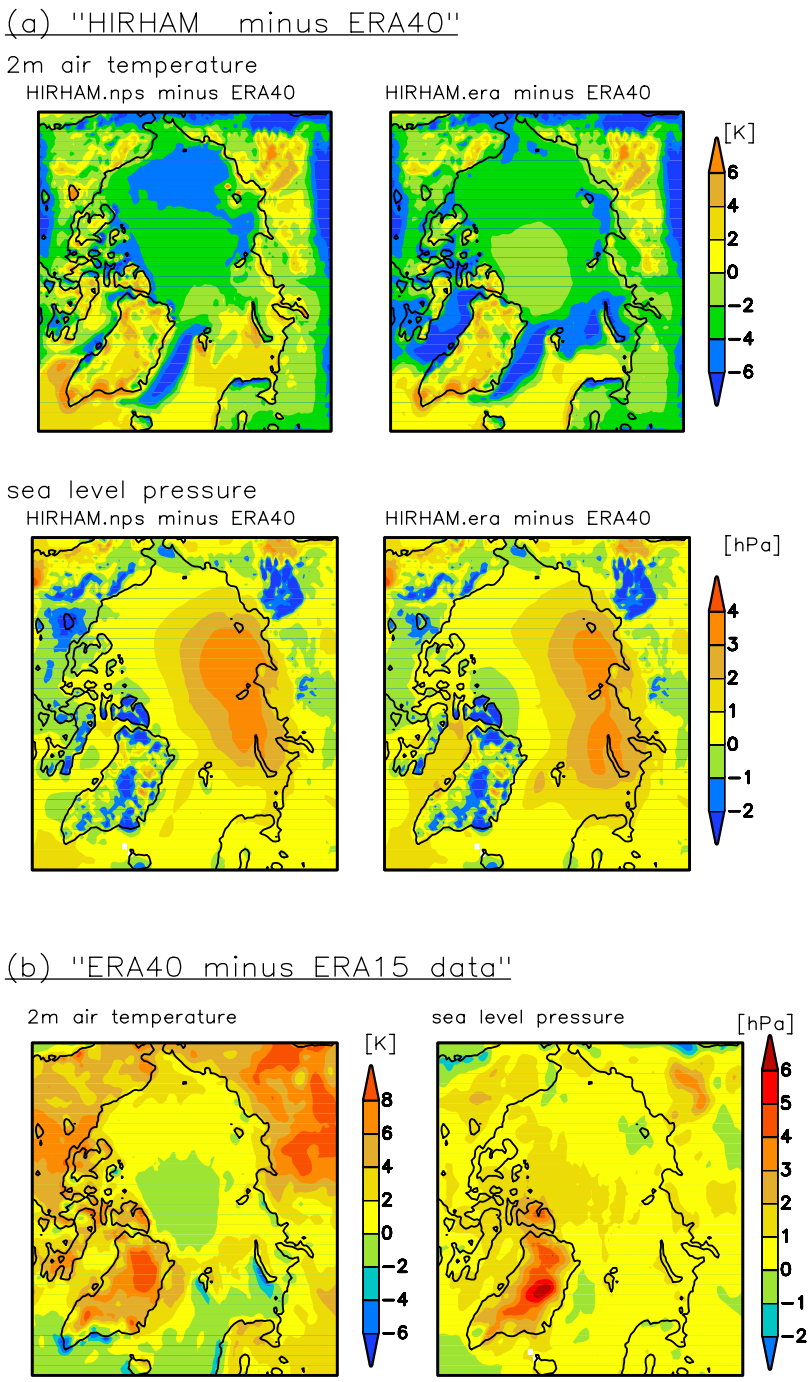

Figure 5. Comparison (a) of the two HIRHAM runs with the ERA40 data and (b) of ERA15 with ERA40 data. The comparisons are shown for the 2 m air temperature and SLP for DJF 1979–1993.

sea ice thickness in the inner Arctic characterized by relatively thick ice (orange and light blue curves) impact the heat fluxes and 2mT much less. The 2mT (SLP) changes there are only about 1/3 (1/10) of those over the marginal ice zone. Interestingly, the sea ice changes affect the atmospheric circulation, namely the SLP, throughout the whole year. During winter (December–April), a clear correlation between 2mT changes and SLP changes is found. Decreased (increased) temperatures generate increased (decreased) SLP, known as the cold high effect. During the rest of the year, the connection of SLP changes to sea ice changes remains unclear.

3.3. Impact on Atmospheric Structure

3.3.1. Atmospheric Temperature Profiles

[24] In contrast to the previous RCM studies this paper also investigates the influence of the lower-boundary forcing on the entire troposphere. It is known that sea ice anomalies can influence the entire atmospheric column by first modifying the boundary layer and then making an impact in the free troposphere (recently, e.g., *Deser et al.*

Table 2. Winter Root-Mean-Square Errors of 2mT and SLP Between the HIRHAM Simulations (HIRHAM.nps, HIRHAM.era) and the Two ECMWF Reanalyses[a]

	2 m Air Temperature, K		Sea Level Pressure, hPa	
Year	HIRHAM.nps	HIRHAM.era	HIRHAM.nps	HIRHAM.era
1979	4.45 (4.00)	4.27 (3.55)	1.97 (4.51)	1.81 (4.80)
1980	3.42 (4.71)	3.51 (4.12)	2.39 (4.01)	1.96 (3.72)
1981	3.68 (4.19)	3.66 (3.77)	2.27 (4.74)	1.34 (4.35)
1982	3.63 (5.06)	3.75 (4.40)	1.75 (4.03)	2.19 (4.57)
1983	3.97 (4.64)	4.08 (3.98)	1.38 (1.97)	1.54 (2.03)
1984	3.92 (5.15)	3.89 (4.69)	1.51 (3.49)	1.64 (3.63)
1985	3.89 (4.44)	3.79 (3.98)	2.27 (3.14)	2.65 (3.33)
1986	3.95 (4.30)	4.15 (3.68)	1.43 (4.57)	1.70 (4.87)
1987	3.58 (4.24)	3.94 (4.00)	1.16 (2.62)	1.62 (2.87)
1988	3.78 (4.26)	4.10 (3.92)	1.90 (3.65)	1.96 (4.47)
1989	3.75 (4.36)	3.94 (4.18)	3.26 (2.22)	3.07 (2.34)
1990	4.16 (4.96)	4.20 (4.47)	1.84 (3.68)	1.50 (3.33)
1991	3.56 (4.52)	3.70 (4.27)	1.26 (3.79)	1.67 (4.48)
1992	3.68 (4.46)	3.48 (3.90)	3.23 (4.02)	2.52 (3.26)
1993	3.89 (4.74)	3.67 (4.02)	2.42 (1.92)	1.68 (2.20)
1979–1993	**3.55 (4.07)**	**3.63 (3.59)**	**1.48 (1.94)**	**1.45 (1.95)**

[a]The values are given using the ERA40 data and in parentheses using the ERA15 data.

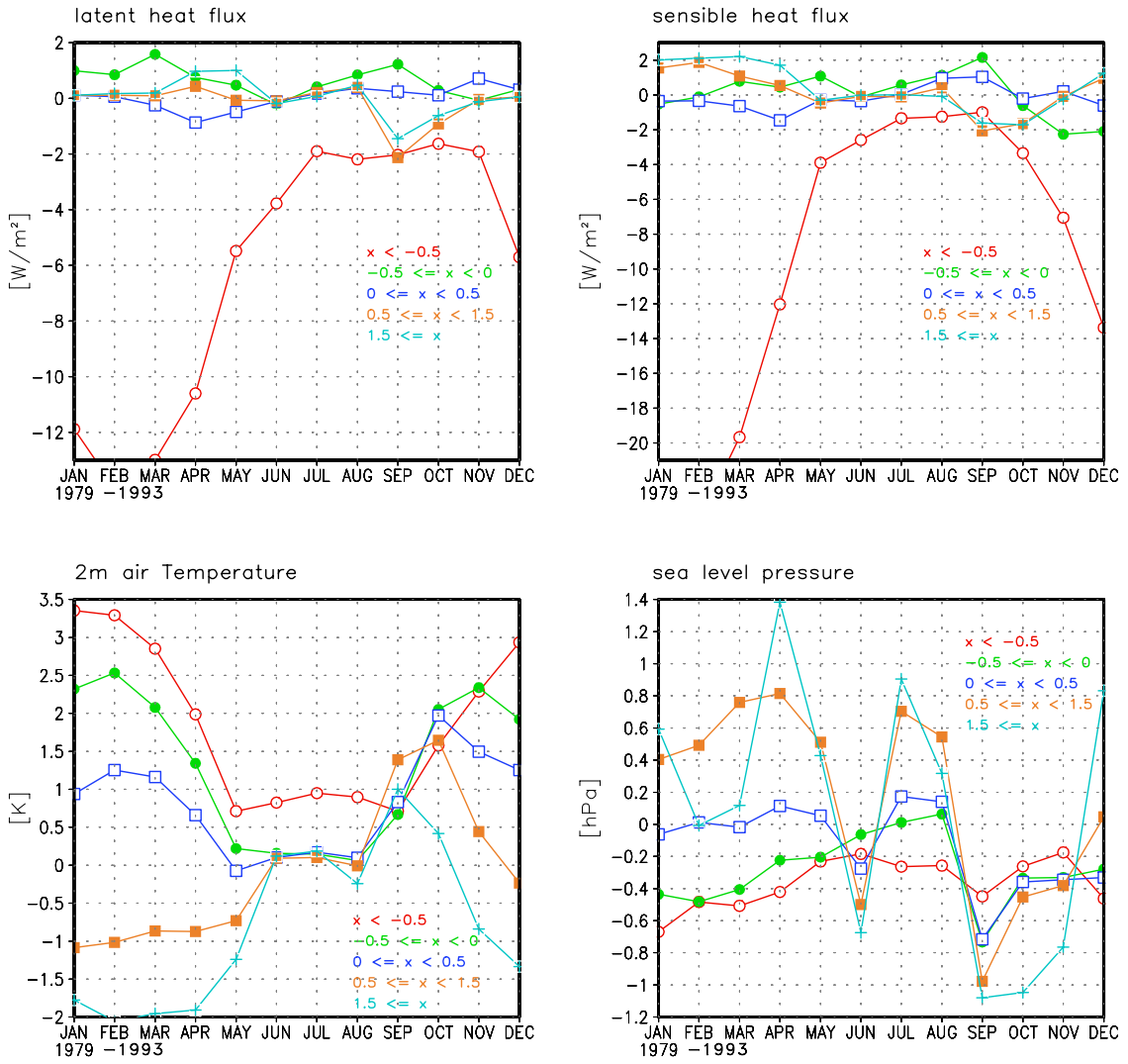

Figure 6. Annual cycle of heat fluxes, 2mT, and SLP differences "HIRHAM.nps minus HIRHAM.era" for several classes x of sea ice thickness differences (in meters).

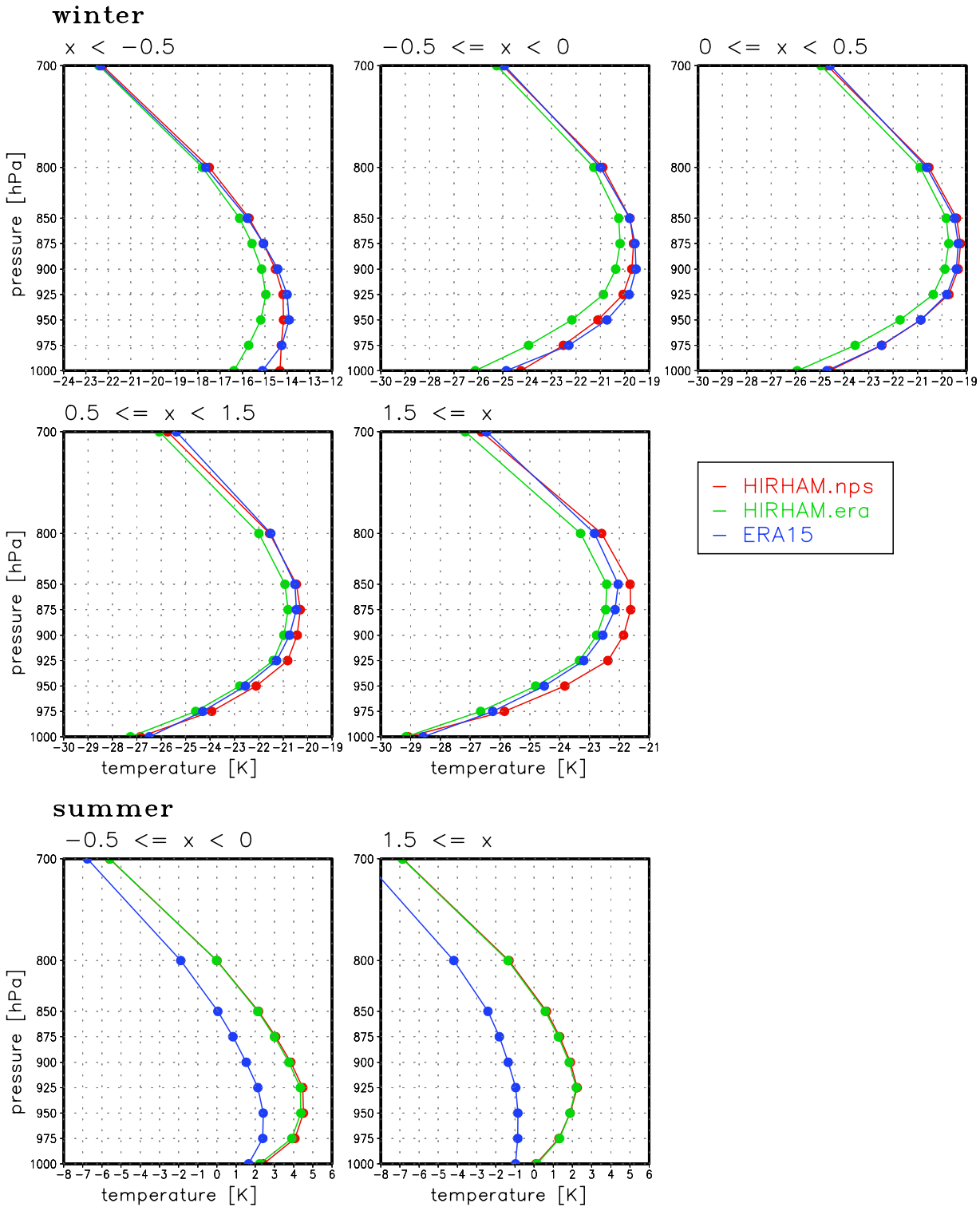

Figure 7. Mean winter (DJF) and mean summer (JJA) vertical temperature profiles of the ERA15 data (blue curves), HIRHAM.nps (red curves), and HIRHAM.era (green curves) for several classes *x* of sea ice thickness differences (in meters).

[2004]). Arctic measurements suggest that a lead width of 10 times the boundary layer height is necessary for the heat flux plume to penetrate the entire boundary layer [*Lüpkes et al.*, 2004].

[25] Figure 7 presents the changes in the vertical temperature profiles associated with the sea ice changes (assigned again to the five classes of ice thickness differences). Comparing the red and green lines (which represent the HIRHAM.nps and HIRHAM.era runs, respectively) it becomes obvious that small (large) ice thickness differences have a large (small) influence on the atmospheric profile in winter. For the 4th class of sea ice changes, the two

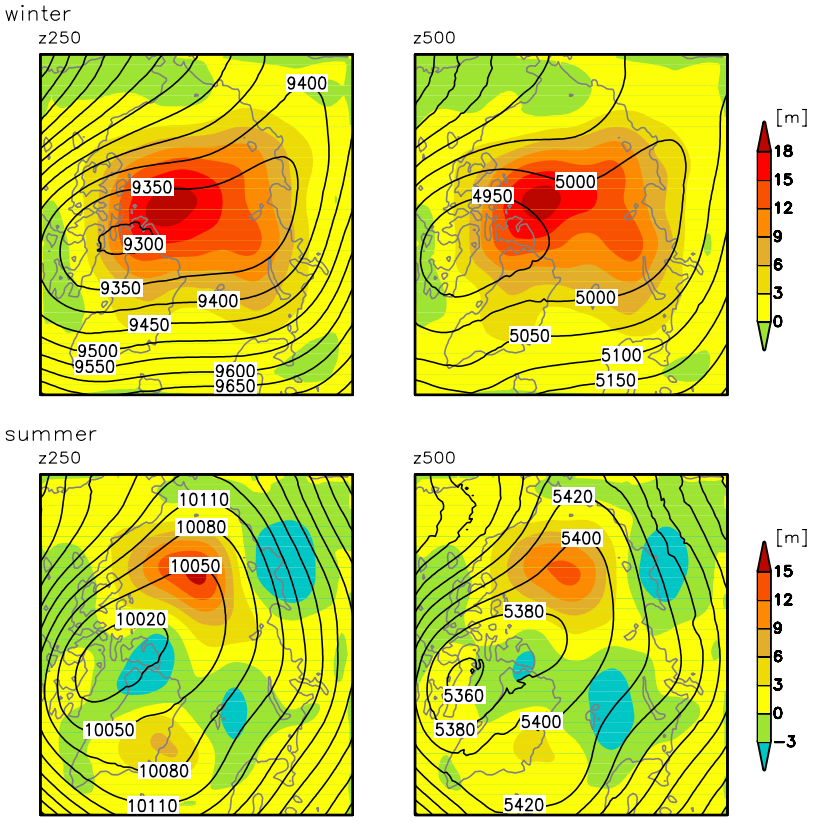

Figure 8. Differences "HIRHAM.nps minus HIRHAM.era" (color shading) and HIRHAM.era (isolines) of geopotential heights at 250 hPa and 500 hPa for DJF and JJA 1979–1993.

HIRHAM simulations do not differ much. So, in regions of relatively thick sea ice (inner Arctic) it seems not absolutely necessary to have the exact ice thickness and its regional distribution to get a reasonable atmospheric temperature profile. A uniform sea ice thickness of 2 m allows for simulation of reasonable air temperature profiles there. In contrast, for the marginal ice zones (classes 1–3), the forcing with the more realistic nps sea ice forcing has an effect on the actual temperature profile in the atmosphere. Consequently, the profiles of the HIRHAM.nps simulation agree quite well with the ERA15 data for the first three classes of sea ice differences, while the HIRHAM.era simulation shows larger deviations. For the last class (i.e., for the region near the Canadian Archipelago), HIRHAM.nps is slightly warmer in the height levels of 950–850 hPa compared to ERA15 data. We assume that this is related to differences in the ice thickness (ERA15 uses 2 m, HIRAM.nps has 3.5–4 m in this region), but it cannot be proven which profile is more realistic due to missing observational data. Further, Figure 7 shows that the impact of the different lower-boundary forcing on the temperature profile over the marginal ice zone is limited to the near-surface layers (1000–850 hPa), while over the thick ice it affects higher layers. Completely different in summer, the different lower-boundary forcing does not significantly influence the atmospheric temperature profiles at all. The profiles by the two HIRHAM simulations do not differ much (but both are warmer than the ERA15 data). This applies for all five classes of sea ice differences; therefore only two of them are shown. This indicates that the use of SST/sea ice from reanalysis and a uniformly prescribed sea ice thickness of 2 m is an acceptable approach for summer simulations in Arctic atmospheric RCMs. Our result confirms the suggestion of *Singarayer et al.* [2005] that the uncertainty in summer sea ice prescription is not critical but that the winter data require greater accuracy. The different seasonal thermodynamic response to sea ice changes can be attributed to the different magnitude of the temperature difference between atmosphere and ocean which is large (small) in winter (summer) associated with large (small) surface heat flux anomalies if sea ice is changing. Thus a high (low) sensitivity of the winter (summer) climate to sea ice changes is apparent.

3.3.2. Spatial Pattern and Profiles of Geopotential

[26] Figure 8 shows that the lower-boundary forcing in winter causes an increase of the 500 hPa geopotential height of about 10–20 m which is of the same order of magnitude as in the recent SST anomaly experiments of *Alexander et al.* [2004] and *Magnusdottir et al.* [2004]. In addition, this magnitude is 1/5–1/3 of the observed interannual SLP variability (calculated from ERA40 data for 1979–2001). The height increase results in a weaker polar vortex in the HIRHAM.nps simulation according to the overall warming of the troposphere shown in Figure 3. The maximum increase of geopotential height occurs over the region of maximum atmospheric warming, i.e., near the Canadian Archipelago. The response in the geopotential height is barotropic, which is in agreement with earlier findings of GCM studies (recently, *Kvamsto et al.* [2004] and

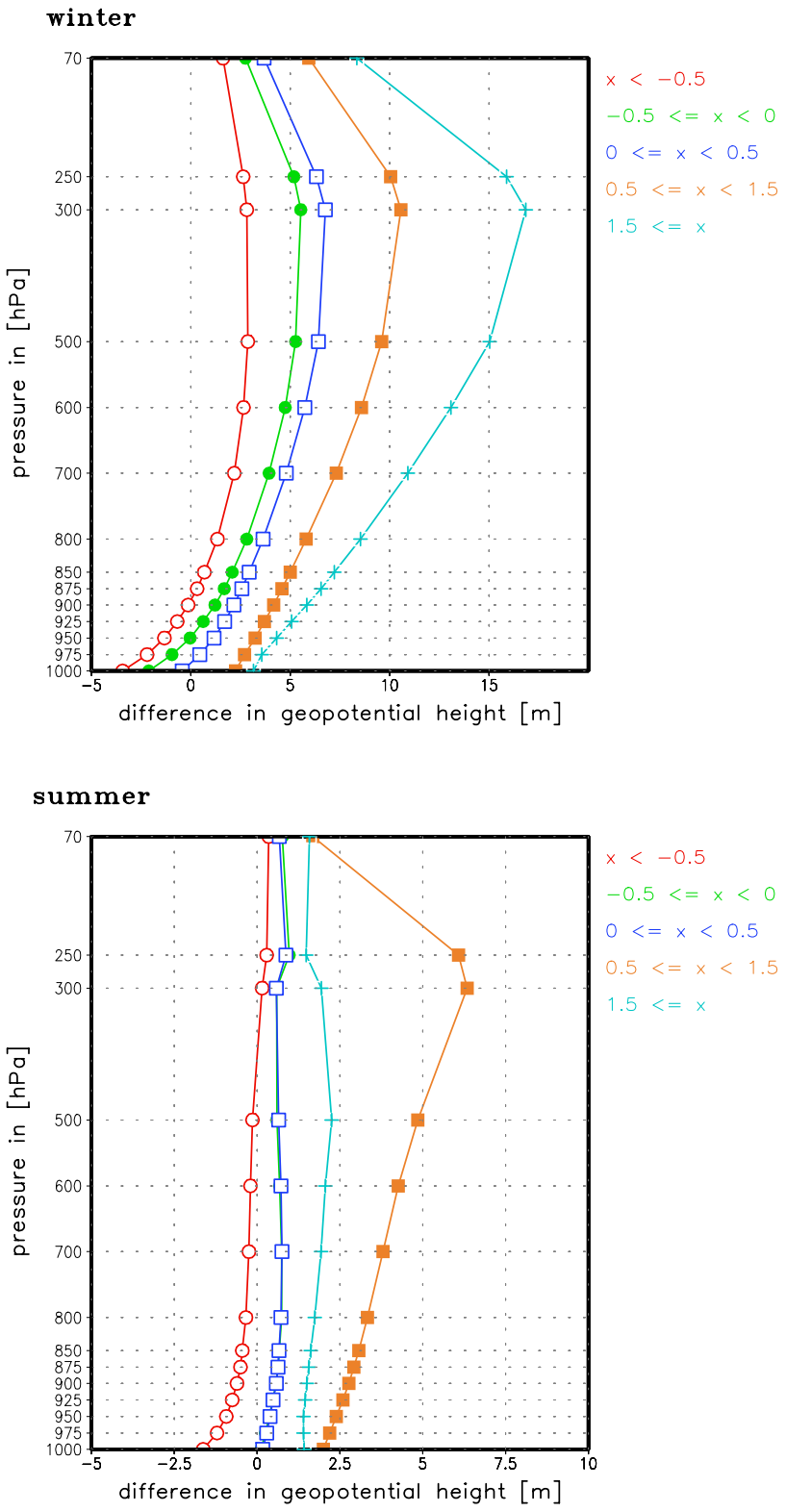

Figure 9. DJF and JJA vertical geopotential height profiles of the difference "HIRHAM.nps minus HIRHAM.era" for several classes x of sea ice thickness differences (in meters).

Alexander et al. [2004]). The geopotential height changes during summer are smaller and show a higher wave number pattern, and the response is also barotropic.

[27] Figure 9 extends the discussion of the dynamic response to the lower-boundary forcing by means of the examination of geopotential profile changes. This is done by considering mean geopotential profiles assigned to the different classes of sea ice thickness changes. Figure 9 indicates that the region of the thickest ice (light blue curve) accounts for the upper tropospheric–lower stratospheric

geopotential response in winter. This region of the western Arctic is the location of maximum atmospheric warming due to the surface direct and indirect forcing and is the center of the vortex. In summer, the impact of the lower-boundary forcing on the atmospheric circulation is generally weaker. However, again, the response is largest in the 250–300 hPa layer and over the western Arctic. Energy fluxes, which excite baroclinic waves are involved in the mechanism of the response and baroclinic instability is widely accepted as the driving mechanism for the high-latitude weather systems. A decrease in the fractional ice cover leads to changes in the surface heat fluxes and a stronger feedback between sea ice and baroclinic weather system development. *Tansley and James* [1999] showed that sea ice exerts a strong influence on the development of baroclinic high-latitude systems. During summer, shorter waves with zonal wave number 3 and weaker amplitudes propagate into the upper troposphere as visible in Figure 8.

4. Summary and Conclusions

[28] The aim of this sensitivity study was to assess the degree to which Arctic atmospheric RCM simulations depend on the ocean boundary forcing and to derive implications for the setup of such simulations. It was shown that the sea ice/SST forcing had an impact on the atmospheric simulations. The main findings can be summarized as follows: The direct thermodynamic response in winter is limited to the near-surface and up to heights of about 800 hPa. The specification of the winter marginal sea ice zone is important for the simulation of regional circulation patterns and atmospheric temperature profiles. A better specification of the thick ice in the western Arctic does not result in advanced atmospheric temperature profiles, however it indicates an Arctic-wide response in the large-scale circulation and seems to have a potential impact on the troposphere-stratosphere coupling. Beside the direct thermodynamic response due to heat flux changes, dynamical responses affect the atmosphere through vertical and horizontal advection. During summer, the thermodynamic effect of sea ice changes is small, but the dynamic response is still of importance yet smaller than in winter.

[29] On the basis of these findings, it is recommended that stand-alone atmospheric RCM simulations specify the SST/sea ice fraction and the spatial distribution of sea ice thickness most realistically in winter, if possible. During summer, this effort is preferable but not as important as in winter. This recommendation goes with the seasonality of the quality of passive microwave satellite-derived sea ice concentrations (quality degrades during summer).

[30] There are important feedbacks between atmosphere and ice/ocean, and these can only be investigated in coupled atmosphere-ice-ocean models. Our experiment with more realistic off-line lower-boundary forcing represents only response in the atmosphere. However, changes in the atmosphere (2mT, SLP, heat fluxes) would yield additional changes in the ice-ocean, which in turn would affect the atmosphere, and so on. One could argue that even small or regional but persistent changes in the atmosphere could result in a significantly different Arctic climate state (i.e., ice-ocean-atmosphere) after some time (e.g., 15 years, if accumulated over that time period). In summary, a fully coupled RCM for the Arctic is needed to comprehensively determine the importance of lower-boundary forcing on simulated climate. However, the range of the nonlinear feedbacks in such coupled model systems makes the understanding of individual processes much more difficult. Therefore the strategy of well-thought investigations with stand-alone models can help to unravel specific relationships and to guide the development of parameterizations of underlying processes responsible for feedbacks between atmosphere and ice/ocean.

[31] **Acknowledgments.** We are grateful to S. Erxleben and I. Hebestadt for programing support and preparing the graphics. A.R. and K.D. were supported by the European Union project "Global implications of Arctic climate processes and feedbacks" (GLIMPSE). W.M. and J.C. were supported by grants from the Office of Polar Programs at the National Science Foundation and by the Climate Change Prediction Program of the Department of Energy. We wish to thank R. Gerdes for useful discussion during the course of this work. The comments from the reviewers improved the manuscript.

References

Alexander, M. A., U. S. Bhatt, J. Walsh, M. Timlin, and J. Miller (2004), The atmospheric response to realistic Arctic sea ice anomalies in an AGCM during winter, *J. Clim.*, *17*, 890–905.

Arctic Climate Impact Assessment (2005), *Arctic Climate Impact Assessment*, 1042 pp., Cambridge Univ. Press, New York.

Bourke, R., and C. Garrett (1987), Sea ice thickness distribution in the Arctic Ocean, *Cold Reg. Sci. Technol.*, *13*, 259–280.

Bourke, R. H., and A. S. McLaren (1992), Contour mapping of Arctic Basin ice draft and roughness parameters, *J. Geophys. Res.*, *97*, 17,715–17,728.

Christensen, J. H., O. B. Christensen, P. Lopez, E. van Meijgaard, and M. Botzet (1996), The HIRHAM4 regional atmospheric climate model, *Sci. Rep. 96-4*, 51 pp., Dan. Meteorol. Inst., Copenhagen.

Clement, J. C., W. Maslowski, L. W. Cooper, J. M. Grebmeier, and W. Walczowski (2005), Ocean circulation and exchanges through the northern Bering Sea—1979—2001 model results, *Deep Sea Res., Part II*, *52*, 3509–3540, doi:10.1016/j.dsr2.2005.09.010.

Deser, C., G. Magnusdottir, R. Saravanan, and A. Phillips (2004), The effects of North Atlantic SST and sea ice anomalies on the winter circulation in CCM3. part II: Direct and indirect components of the response, *J. Clim.*, *17*, 877–889.

Dethloff, K., A. Rinke, R. Lehmann, J. H. Christensen, M. Botzet, and B. Machenhauer (1996), A regional climate model of the Arctic atmosphere, *J. Geophys. Res.*, *101*, 23,401–23,422.

Dethloff, K., W. Dorn, A. Rinke, K. Fraedrich, M. Junge, E. Roeckner, V. Gayler, U. Cubasch, and J. H. Christensen (2004), The impact of Greenland's deglaciation on the Arctic circulation, *Geophys. Res. Lett.*, *31*, L19201, doi:10.1029/2004GL020714.

Dethloff, K., et al. (2006), A dynamical link between the Arctic and the global climate system, *Geophys. Res. Lett.*, *33*, L03703, doi:10.1029/2005GL025245.

Dukowicz, J. K., and R. D. Smith (1994), Implicit free-surface method for the Bryan-Cox-Semtner ocean model, *J. Geophys. Res.*, *99*, 7991–8014.

Fowler, C., J. Maslanik, T. Haran, T. Scambos, J. Key, and W. Emery (2002), AVHRR Polar Pathfinder twice-daily 25 km EASE-Grid composites, http://nsidc.org/data/nsidc-0094.html, Natl. Snow and Ice Data Cent., Boulder, Colo.

Gibson, J. K., P. Kallberg, S. Uppala, A. Noumura, A. Hernandez, and E. Serrano (1997), ERA description, *ECMWF Reanalysis Proj. Rep. Ser. 1*, 77 pp., ECMWF, Reading, U. K.

Görgen, K. (2004), Sensitivitätsstudien und Analyse von Atmosphäre-Meereis- Wechselwirkungen mit dem regionalen Atmosphärenmodell HIRHAM4 auf Basis eines neu entwickelten beobachtungsgestützten unteren Modellantriebs während ausgewählter Sommer über der Arktis/Laptewsee, Ph.D. dissertation, Univ. of Trier, Germany.

Grønas, S. (1995), The seclusion intensification of the New Year's day storm 1992, *Tellus, Ser. A*, *47*, 733–746.

Harms, I. H., C. Schrum, and K. Hatten (2005), Numerical sensitivity studies on the variability of climate-relevant processes in the Barents Sea, *J. Geophys. Res.*, *110*, C06002, doi:10.1029/2004JC002559.

Hoskins, B. J., M. E. McIntyre, and A. W. Robertson (1985), On the use and significance of isentropic potential vorticity maps, *Q. J. R. Meteorol. Soc.*, *111*, 877–946.

Kushnir, Y., W. A. Robinson, I. Blad, N. M. J. Hall, S. Peng, and R. Sutton (2002), Atmospheric GCM response to extratropical SST anomalies: Synthesis and evaluation, *J. Clim.*, *15*, 2233–2256.

Kvamsto, N. G., P. Skeie, and D. B. Stephenson (2004), Impact of Labrador sea-ice on the North Atlantic Oscillation, *Int. J. Climatol.*, *24*, 603–612.

Lopez, P., T. Schmith, and E. Kaas (2000), Sensitivity of the Northern Hemisphere circulation to North Atlantic SSTs in the ARPEGE climate AGCM, *Clim. Dyn.*, *16*, 535–547.

Lüpkes, C., J. Hartmann, G. Birnbaum, W. Cohrs, M. Yelland, R. Pascal, T. Spiess, and M. Buschmann (2004), Convection Over Arctic Leads (COAL), *Rep. Polar Res. 481*, pp. 47–62, Alfred Wegener Inst. for Polar and Mar. Res., Bremerhaven, Germany.

Magnusdottir, G., C. Deser, and R. Saravanan (2004), The effects of North Atlantic SST and sea-ice anomalies on the winter circulation in CCM3. part 1: Main features and storm-track characteristics of the response, *J. Clim.*, *17*, 857–876.

Maslowski, W., and W. H. Lipscomb (2003), High resolution simulations of Arctic sea ice, 1979–1993, *Polar Res.*, *22*, 67–74.

Maslowski, W., B. Newton, P. Schlosser, A. Semtner, and D. Martinson (2000), Modeling recent climate variability in the Arctic Ocean, *Geophys. Res. Lett.*, *27*, 3743–3746.

Maslowski, W., D. C. Marble, W. Walczowski, and A. J. Semtner (2001), On large scale shifts in the Arctic Ocean and sea ice conditions during 1979–1998, *Ann. Glaciol.*, *33*, 545–550.

Maslowski, W., D. Marble, W. Walczowski, U. Schauer, J. L. Clement, and A. J. Semtner (2004), On climatological mass, heat, and salt transports through the Barents Sea and Fram Strait from a pan-Arctic coupled ice-ocean model simulation, *J. Geophys. Res.*, *109*, C03032, doi:10.1029/2001JC001039.

Matishov, G. G., V. A. Volkov, and V. V. Denisov (1998), On the structure of the warm Atlantic waters circulation in the northern part of the Barents Sea, *Dokl. Akad. Nauk*, *362*, 553–556.

Oberhuber, J. M. (1992), The OPYC ocean general circulation model, *Tech. Rep. 7*, Dtsch. Klimarechenzent., Hamburg, Germany.

Paeth, H., M. Latif, and A. Hense (2003), Global SST influence on twentieth century NAO variability, *Clim. Dyn.*, *21*, 63–75.

Preller, R. H., W. Maslowski, P. G. Posey, D. Stark, and T. T. C. Pham (2002), Navy sea ice prediction systems, *Oceanography*, *15*, 44–56.

Rinke, A., and K. Dethloff (2000), On the sensitivity of a regional Arctic climate model to initial and boundary conditions, *Clim. Res.*, *14*, 101–113.

Rinke, A., K. Dethloff, and M. Fortmann (2004a), Regional climate effects of Arctic Haze, *Geophys. Res. Lett.*, *31*, L16202, doi:10.1029/2004GL020318.

Rinke, A., P. Marbaix, and K. Dethloff (2004b), Internal variability in Arctic regional climate simulations: Case study for the SHEBA year, *Clim. Res.*, *27*, 197–209.

Roeckner, E., et al. (1996), The atmospheric general circulation model ECHAM4: Model description and simulation of present-day climate, *Rep. 218*, 90 pp., Max Planck Inst., Hamburg, Germany.

Semmler, T., D. Jacob, K. H. Schluenzen, and R. Podzun (2004), Influence of sea ice treatment in a regional climate model on boundary layer values in the Fram Strait region, *Mon. Weather Rev.*, *132*, 985–999.

Singarayer, J. S., P. J. Valdes, and J. L. Bamber (2005), The atmospheric impact of uncertainties in recent Arctic sea ice reconstructions, *J. Clim.*, *18*, 3996–4012.

Steele, M., R. Morfley, and W. Ermold (2001), PHC: A global ocean hydrography with a high- quality Arctic Ocean, *J. Clim.*, *14*, 2079–2087.

Tansley, C. E., and I. N. James (1999), Feedbacks between sea ice and baroclinic waves using a linear quasi-geostrophic model, *Q. J. R. Meteorol. Soc.*, *125*, 2517–2534.

Viterbo, P., and A. K. Betts (1999), The impact on ECMWF forecasts of changes to the albedo of the boreal forests in the presence of snow, *J. Geophys. Res.*, *104*, 27,803–27,810.

Wu, B., J. Wang, and J. Walsh (2004), Possible feedback of winter sea ice in the Greenland and Barents Seas on the local atmosphere, *Mon. Weather Rev.*, *132*, 1868–1876.

Zhang, J., M. Steele, D. A. Rothrock, and R. W. Lindsay (2004), Increasing exchanges at Greenland-Scotland Ridge and their links with the North Atlantic Oscillation and Arctic sea ice, *Geophys. Res. Lett.*, *31*, L09307, doi:10.1029/2003GL019304.

Zhang, Y., W. Maslowski, and A. J. Semtner (1999), Impact of mesoscale ocean currents on sea ice in high-resolution Arctic ice and ocean simulations, *J. Geophys. Res.*, *104*, 18,409–18,429.

J. Clement and W. Maslowski, Department of Oceanography, Naval Postgraduate School, 833 Dyer Road, Monterey, CA 93943, USA.

K. Dethloff and A. Rinke, Alfred Wegener Institute for Polar and Marine Research, Telegrafenberg A43, D-14473 Potsdam, Germany. (arinke@awi-potsdam.de)